◎ 논 문
◎ Original Paper

DOI: https://doi.org/10.5293/kfma.2024.27.3.054
ISSN (Print): 2287-9706

펌프수차 수차모드 운전 시 S-곡선 영역에서 임펠러 블레이드 각도의 영향

쉬레스트 우즈왈* · 최영도**†

Effect of Pump Turbine Impeller Blade Angle in the S-Curve Region While Operating in Turbine Mode

Ujjwal Shrestha*, Young-Do Choi**†

Key Words : Pump-Turbine(펌프수차), Performance(성능), S-Curve(S-곡선), Blade angle(블레이드 각도), Turbine mode(수차모드)

ABSTRACT

Pump turbine demand is increasing for the energy storage system. The pump turbine continuously needs to switch between pump mode and turbine mode. When the pump turbine operates at a partial flow rate in the turbine mode, it shows the unsteady S-Curve region. The recirculation flow and vortexes persist in the S-Curve region, which causes a blockage, stall, and pressure fluctuation in the pump turbine. Furthermore, the impeller shape plays a vital role in the contribution of the S-Curve. In this study, the inlet blade angle (β_2) in turbine mode was selected as a geometrical parameter to study its effect on hydraulic performance in the S-Curve region of the pump turbine model. The higher value of β_2 increases the magnitude of inward radial velocity to decrease vortexes and recirculation flow in the S-Curve region. Hence, the higher β_2 is suitable for reducing vortexes and recirculation flow in the S-Curve region.

1. Introduction

The increase in renewable energy production causes a surge in the energy storage demand. The ability to store electricity from the renewable energy source is the main problem. The pump turbine is a reliable technique for electricity storage from renewable energy sources[1]. According to the International Hydropower Association, the pump storage capacity reached 175 GW in 2022, which increased by 6% from 2021[2]. The demand for pump storage systems is increasing to supply stable renewable energy. The pump turbine continuously operates from pump mode to turbine mode. In pump mode, the pump turbine operates as a pump to store water from the lower reservoir to the upper reservoir. It uses water from the upper reservoir to generate high-grade electricity in turbine mode. The pump turbine often operates in off-design conditions. The pump turbine design comprises the performance of pump mode and turbine mode, regulatory capacity, and cavitation. The design criteria of the pump turbine focused on the pump mode operation. When the pump turbine operates at off-design conditions in turbine mode, the unstable region will appear with recirculation flow in the blade passage. Pejovic et al.[3] and Dörfler et al.[4] explained the stability problems during start-up in turbine mode, load rejection, and low head operation.

The pump turbine operation at the unstable region is called an S-Curve region. In the S-Curve region, the

* Graduate School, Department of Mechanical Engineering, Mokpo National University
** Department of Mechanical Engineering, Institute of New and Renewable Energy Technology Research, Mokpo National University
† 교신저자, E-mail : ydchoi@mnu.ac.kr

pump turbine experiences a sudden change of torque and pressure fluctuations, which causes self-excited vibrations[5]. The vortexes, recirculation flow, and eddies are developed in the impeller flow passage at the S-Curve region[6-8]. The development of a vortex in the S-Curve region causes the flow blockage. Zhang et al. experimented using PIV to conclude that the large-scale vortex appeared at the leading edge of the impeller in turbine mode[9]. The flow blockage in the S-Curve region due to the vortexes causes high-pressure fluctuations and stalls in blade passages[10]. Senoo[11] and Olimstad[12] showed the unstable S-Curve characteristics curve of pump turbines at no-flow and turbine mode operation, respectively.

Zanetti performed the numerical analysis in the low-specific speed pump turbine to characterize the flow field to the slope variation of the S-Curve[13]. Jin et al. used 1D-3D coupled CFD analysis to identify the precise location of flow energy dissipation in the pump turbine during turbine mode[14]. The pump impeller with a negative outlet velocity moment can decrease hydraulic loss in the draft tube and improve the pump as a turbine performance[15]. The numerical investigation suggests that the centrifugal pump with a splitter blade can reduce flow irregularities when operating in turbine mode[16]. The effects of splitter blade geometry on the performance curve and S-shape characteristics of pump turbines in turbine modes are examined by numerical simulation[17].

The main characteristics of the hydraulic instabilities are caused by one or more geometrical parameters[18]. The parametric studies of blade number, blade angles, and impeller diameter are required to detail understanding of the pump turbine flow dynamics. The impeller blade angles, diameters, and width influenced the S-Curve nature. Few studies about the impeller blade angle effects on the S-Curve are available, but the results are inconclusive. Hence, the blade inlet angle in turbine mode is selected for the detailed understanding of flow dynamics and the S-Curve region.

2. Design and Methodology

2.1 Design of scale down pump turbine model

The pump turbine model is used for performance investigation and internal flow analysis. The specific speed of the pump turbine is 31 [m-m^3/s] and 105 [m-kW] at pump mode and turbine mode, which are calculated using Eqs. (1) and (2), respectively[19].

$$n_{sp_P} = \frac{N\sqrt{Q_P}}{H_P^{0.75}} \tag{1}$$

$$n_{sp_T} = \frac{N\sqrt{P_T}}{H_T^{1.25}} \tag{2}$$

where, n_{sp} specific speed of the pump turbine. N, Q, H, and P are rotational speed (min^{-1}), flow rate (m^3/s), effective head (m) and output power (kW). The subscript P, and T represent the pump and turbine modes, respectively.

The pump turbine operates at the same rotational speed of 1800 min^{-1} for both pump and turbine modes. The head and flow rate values for the pump and turbine modes are H_P = 16.5 m, Q_P = 0.020 m^3/s, and H_T = 15 m, Q_T = 0.026 m^3/s, respectively. The design of the pump turbine is accomplished with the background theory of gradient of flow variation to head variation[20]. The meridional shape of the pump turbine is shown in Fig. 1, and the flow direction is according to the turbine mode. The meridional shape for a low

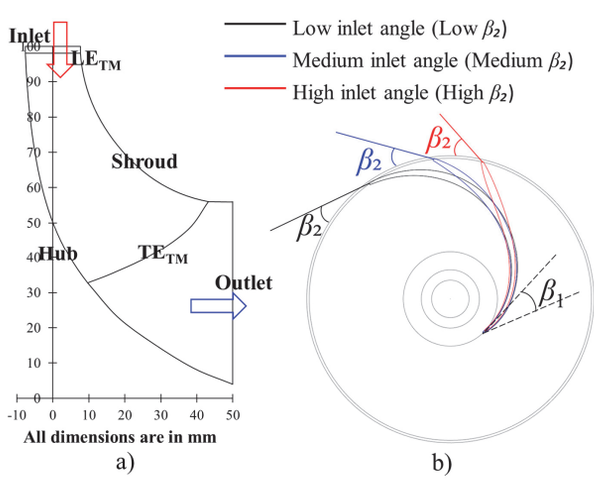

Fig. 1 a) Meridional shape and b) plane view of pump turbine in turbine mode

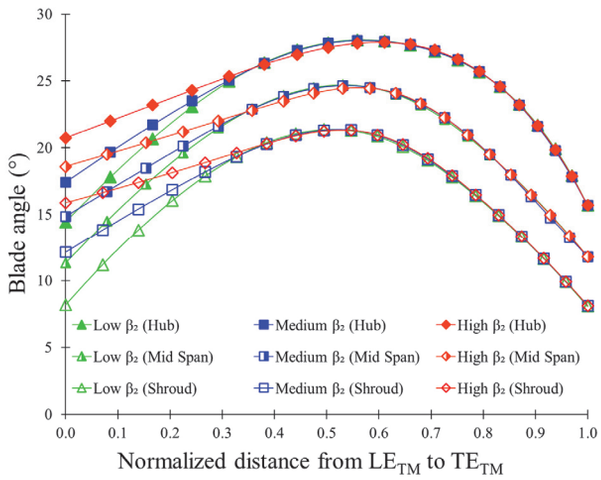

Fig. 2 Blade angle distribution of impeller at hub, mid span and shroud in turbine mode

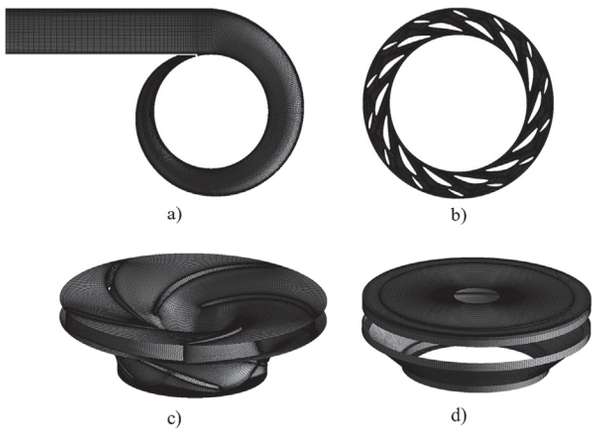

Fig. 3 Numerical grids of pump turbine model a) casing, b) stay vane and guide vane, c) impeller and d) clearance gap

specific speed pump turbine is shown in Fig. 1. The inlet and outlet diameters of the pump turbine are 198 mm and 112 mm, respectively, in turbine mode. The outlet width of the pump turbine impeller is 15.2 mm. The pump turbine diameter is considerably small, and leakage loss is prominent. The number of impeller blades is 5 and 14 guide and stay vanes each. The inlet and outlet locations are interchangeable with the pump and turbine modes in the pump turbine. β_1 and β_2 are inlet and outlet blade angles for the pump turbine in pump mode, respectively. The inlet and outlet blade angles are β_2 and β_1, respectively, in the turbine mode of a pump turbine.

Fig. 2 shows the blade angle distribution from LE$_{TM}$ to TE$_{TM}$ at the hub and shroud in the pump turbine. The blade angle β_2 increases linearly from hub to shroud at LE$_{TM}$. The inlet angle is changed from 13° to 22°, 11° to 19° and 7° to 16° at the hub, mid span, and shroud, respectively, in turbine mode.

2.2 Numerical methodology

ANSYS 2022R2[21] is used for CFD analysis of pump turbines in which Reynolds-averaged Navier-Stokes equations are used to solve steady incompressible simulations. The numerical grids play a vital role in CFD analysis. The hexahedral grids were generated using ANSYS 2022R2 ICEM[21]. The numerical grids for the casing, stay vanes, guide vanes, impeller, and clearance gap are shown in Fig. 3. CFD analysis is critically dependent on the numerical grids. The mesh

Table 1 Discretization error for the numerical solution

	Efficiency	
	Pump Mode	Turbine Mode
G_1, G_2, G_3	13.2×10^6, 6.6×10^6, 2.4×10^6	
r_{21}	1.26	
r_{32}	1.40	
η_1	83.60	85.22
η_2	84.10	86.48
η_3	83.95	86.19
p_0	5.26	6.42
η_{ext}^{21}	83.39	84.84
ϵ_a^{21}	0.0060	0.0148
ϵ_{ext}^{21}	0.0026	0.0044
GCI_{fine}^{21}	0.32%	0.55%
GCI_{fine}^{32}	0.05%	0.06%

dependency test was conducted to obtain the optimal grid numbers for the stable CFD analysis results. Grid convergence test is carried out with grid sizes G_1, G_2, and G_3 using grid convergence index (GCI). The efficiencies at pump and turbine modes are selected for the sensitivity analysis. GCI is calculated using Eq. (3)[22].

$$GCI_{fine}^{21} = \frac{1.25\epsilon_a^{21}}{r_{21}^{p_0}-1} \tag{3}$$

where G is grid number, η is efficiency, ϵ is the relative error, r is the grid refinement factor, p_0 is the apparent order of numerical solution, the subscript a and ext are approximate and extrapolated relative error values, respectively.

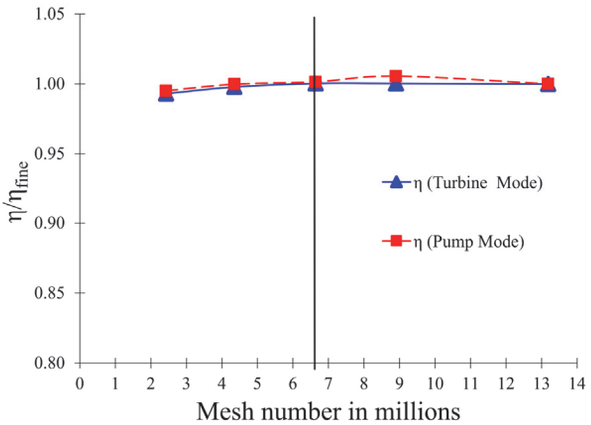

Fig. 4 Grids dependency test for pump turbine analysis

Table 1 shows the discretization error analysis for CFD analysis. *GCI* is less than 1% for both pump and turbine efficiencies. Fig. 4 shows the mesh dependency test conducted for turbine and pump modes. The mesh dependency test indicated that 6.7 million nodes are suitable for the stable CFD analysis results. Besides numerical grids, the proper boundary is required for accurate numerical analysis. The pump turbine operates in both turbine and pump modes and requires separate boundary conditions for each operation. For turbine mode, the inlet and outlet are total pressure and static pressure, respectively[23]. In turbine mode, the guide vane opening controls the flow rate. Similarly, in pump mode, the inlet is static pressure, and the outlet is mass flow rate[24].

Furthermore, the RANS equation with the shear stress transport (SST) model is used to solve simulations of the pump turbine in turbine and pump modes. The full-domain pump turbine was used to perform CFD analysis. The frozen rotor was selected for the interface between stationary and rotating components. The high-resolution scheme is chosen for the advection scheme and turbulence numeric. The residual root mean square value for the convergence criteria is 10^{-6}. The summarized boundary conditions for turbine and pump modes are shown in Table 2. For the analysis of the S-Curve region, the outlet of turbine mode is replaced from static pressure to mass flow rate. The S-Curve is obtained by decreasing the mass flow rate at the same guide vane opening. The mass flow rate at the turbine mode is reduced gradually to observe the S-Curve region at a partial flow rate. For reverse pump mode analysis, the inlet and outlet locations are reversed while keeping the impeller rotation direction the same as in turbine mode.

Table 2 Boundary conditions for pump turbine analysis

Specification	Turbine	Pump
Inlet	Total Pressure	Static Pressure
Outlet	Static Pressure	Mass Flow Rate
Turbulence Model	Shear Stress Transport	
Interface Model	Frozen Rotor	
Reference Pressure	1 atm	
Wall Condition	No Slip Wall	

3. Results and Discussion

3.1 Performance curves of pump turbine

The performance curves for the pump turbine in pump and turbine modes with leakage flow were obtained using CFD analysis. Fig. 5 shows the performance curves of the pump turbine in pump mode. The best efficiency of 84% and head of 15m is achieved in pump mode. Generally, the design of the pump turbine is considered with pump mode performance curves. The best efficiency point matches the design point in pump mode. Hence, the design of the pump turbine is acceptable. At partial flow rate, the high β_2 shows marginally better efficiency than the medium and low β_2 pump turbine impeller. However, at a high flow rate, the difference in efficiency and head

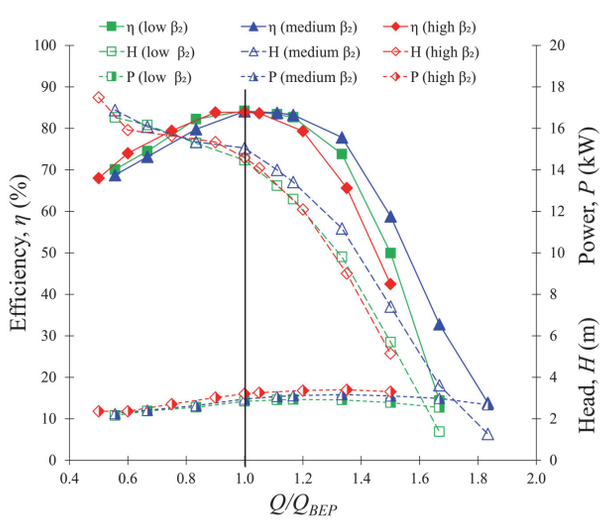

Fig. 5 Performance curves of pump turbine in pump mode

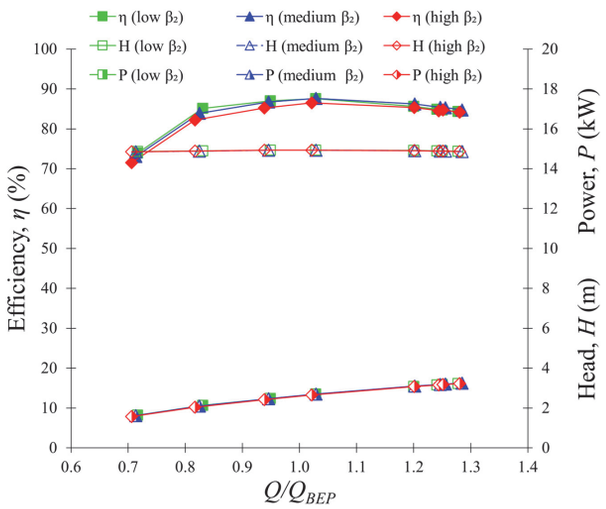

Fig. 6 Performance curves of pump turbine in turbine mode

of the pump turbine in pump mode is visible in Fig. 5. The efficiency and head of the pump turbine in pump mode are better in medium β_2 impeller than high and low β_2 impeller. The high β_2 impeller showed higher input power and low head. Hence, Fig. 5 shows that medium β_2 shows better performance of the pump turbine in pump mode.

Fig. 6 shows the performance curves of the pump turbine in turbine mode. The performance curves of the pump turbine are approximately similar to β_2 variation in turbine mode. The best efficiency of the scale-down pump turbine model in turbine mode is 88% at the medium β_2. The constant head of 15m is reached in turbine mode. The performance curves of the pump turbine showed that the efficiency, head, and output power are approximately the same with the variation of impeller β_2.

3.2 Internal flow of pump turbine in turbine mode

Pump turbine design focused on the pump mode performance. Therefore, flow irregularities and secondary flow occurrences in the impeller flow passage are usual in turbine mode operation. Fig. 7 shows the blade loading of the pump turbine model in turbine mode. The pressure distribution at the pressure side increases with a rise in flow rate. The pressure at the trailing edge in turbine mode is higher than atmospheric pressure, which suggests that the

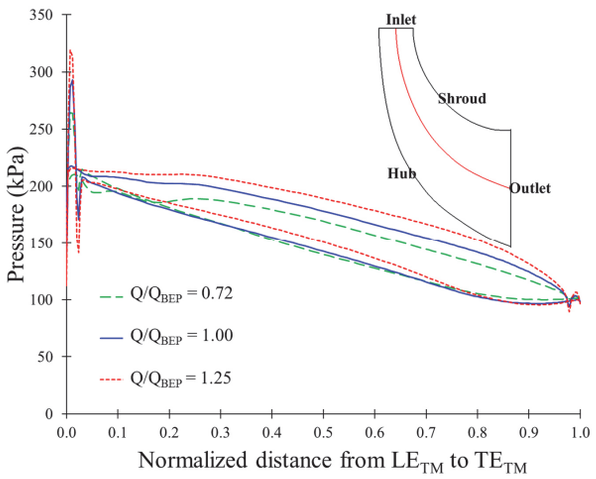

Fig. 7 Blade loading at various flow rate in medium β_2 in turbine mode

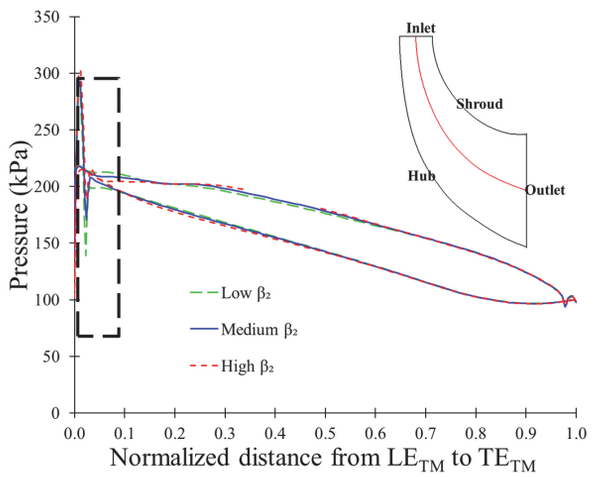

Fig. 8 Blade loading at Q/Q_{BEP}=1.00 various β_2 in turbine mode

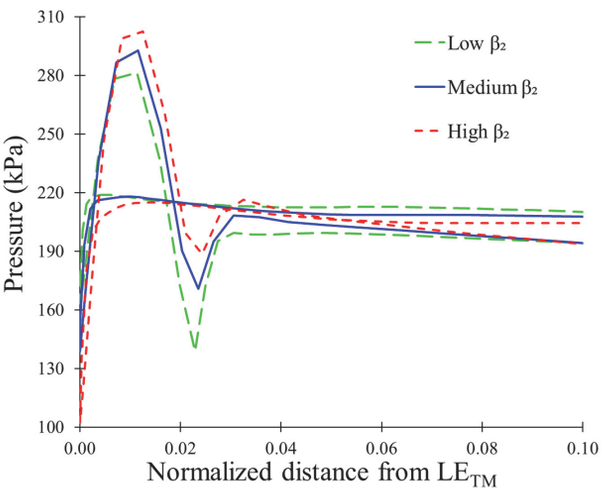

Fig. 9 Magnify view of fig. 8 blade loading at Q/Q_{BEP} = 1.00 various β_2 in turbine mode

possibility of cavitation is low in the turbine at various flow conditions. The crossover between the pressure and suction sides is avoided in the current design of the pump turbine in turbine mode. Hence, the design of the pump turbine in turbine mode is acceptable.

Fig. 8 shows the blade loading at Q/Q_{BEP}=1.00 with various β_2 in turbine mode. The pressure distribution in the impeller blade with various β_2 is approximately the same from a normalized distance of 0.1–1.0. The magnified view of Fig. 8, at a normalized distance from 0.0–0.1, is shown in Fig. 9. The sudden rise in the pressure is observed at the leading edge (LE).

The high β_2 showed a comparatively high-pressure rise than medium and low β_2. At 0.02 normalized distance from LE, a sudden drop of pressure occurred. The pressure drop for high, medium, and low β_2 are 113 kPa, 122 kPa, and 142 kPa, respectively. These pressure drops at the LE cause shock loss in the pump turbine at turbine mode. The high β_2 reduces the pressure drop at LE, which eventually reduces the shock loss and improves the S-Curve region in the pump turbine at turbine mode.

Fig. 10 shows the pressure distribution from the hub to the shroud at LE of the impeller in turbine mode. The difference in the pressure distribution from hub to shroud is observed with low, medium, and high β_2 in turbine mode. The low β_2 impeller has a lower pressure value than the medium and high β_2 impeller in turbine mode. It implies that pressure at the inlet increases

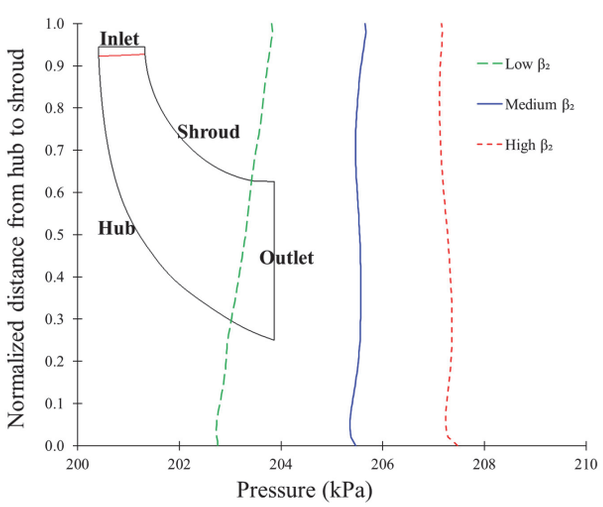

Fig. 10 Pressure distribution from hub to shroud at Q/Q_{BEP} = 1.00 with various β_2 in turbine mode

with β_2 in turbine mode. The pressure distribution from hub to shroud in medium and high β_2 is constant and linear, but with low β_2, the pressure distribution is non-linear. The pressure difference is observed at the hub and shroud in the impeller with low β_2, which leads to recirculation flow and shock loss. The higher value β_2 is preferable for constant and linear pressure distribution at LE from hub to shroud in turbine mode.

3.3 Effect of blade angle on S-Curve region

The S-Curve region is prepared with a change in the flow rate in turbine mode. The unit discharge and unit speed are used to evaluate the S-Curve region.

$$N_{11} = \frac{ND}{\sqrt{H}} \tag{4}$$

$$Q_{11} = \frac{Q}{D^2\sqrt{H}} \tag{5}$$

where N, Q, H, and P are rotational speed (min^{-1}), flow rate (m^3/s), effective head (m), and output power (kW), respectively. D is outlet diameter according to turbine mode.

Fig. 11 shows the variation in the S-Curve region according to β_2 in turbine mode. The S-Curve region occurred at Q_{11} from 0.02–0.20 and N_{11} from 60–65. In turbine mode, the S-Curve region is influenced by head and flow rate. The β_2 variation shows the difference in the S-Curve region. The S-Curve begins at Q_{11}=0.19, 0.21, 0.18, and N_{11}=65.04, 63.81, 63.91 for low, medium, and high β_2, respectively. The S-Curve ends at Q_{11}=0.05, 0.05, 0.05, and N_{11}=63.41, 62.70, 61.92 for low, medium, and high β_2, respectively. The variation in Q_{11} and N_{11} changes the inclination of the S-Curve. The low β_2 causes the steeper S-Curve region compared to medium and high β_2. For medium and high β_2, the S-Curve region begins from the same point, but the S-Curve region for the high β_2 ends at a lower value of Q_{11} and N_{11}. It implies that the steepness of the S-Curve for high β_2 is much steeper than medium β_2. However, the low β_2 has approximately the same ending point of the S-Curve region with medium β_2, but the beginning of the S-Curve region has a high value of Q_1 and N_{11}.

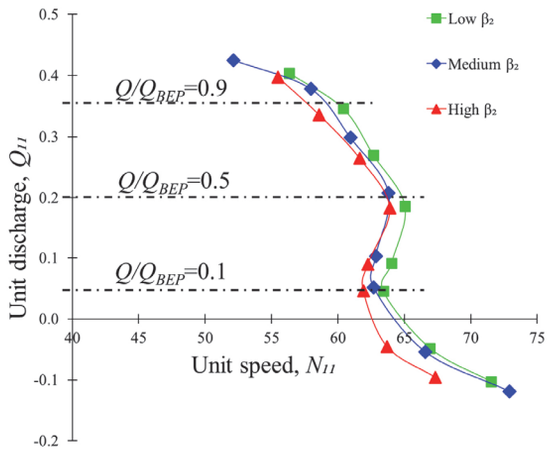

Fig. 11 S–Curve region in the pump turbine with various β_2 impeller

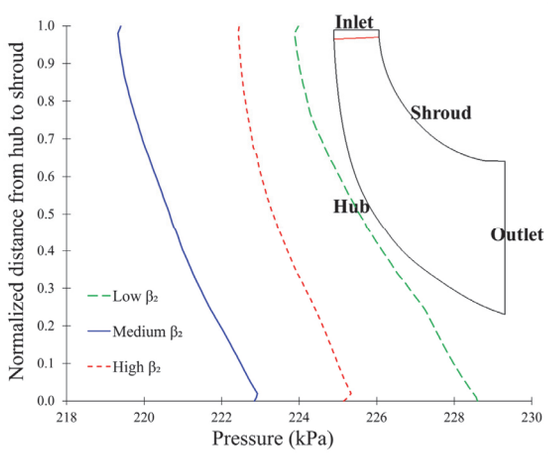

Fig. 12 Pressure distribution from hub to shroud at Q/Q_{BEP} = 0.10 of S–Curve region with various β_2 impeller in turbine mode inlet

Hence, the S–Curve regions from Q_{11}=0.20–0.05, low and high β_2 are steeper than medium β_2. The steepness of the S–Curve region increases the vortexes and recirculation flow in the blade passage.

Fig. 12 shows the pressure distribution from hub to shroud at Q/Q_{BEP}=0.10 in turbine mode inlet. The pressure distribution shows the inclination from hub to shroud in the S–Curve region compared to standard operation in turbine mode. The pressure difference from hub to shroud causes the recirculation flow and vortexes in the turbine mode inlet.

Fig. 13 shows the velocity vectors Q/Q_{BEP}=0.90 of the S–Curve region in turbine mode. The velocity vectors are smooth without any recirculation and eddies flow. The low, medium, and high β_2 have a smooth flow from

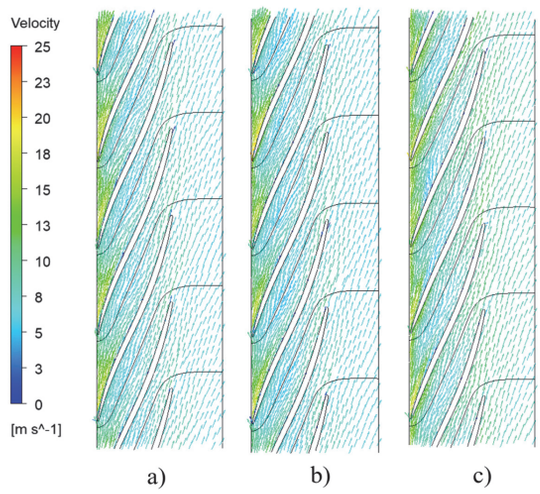

Fig. 13 Velocity vectors in impeller flow passage a) low β_2, b) medium β_2 and c) high β_2 at Q/Q_{BEP} = 0.90 of S–Curve region in turbine mode

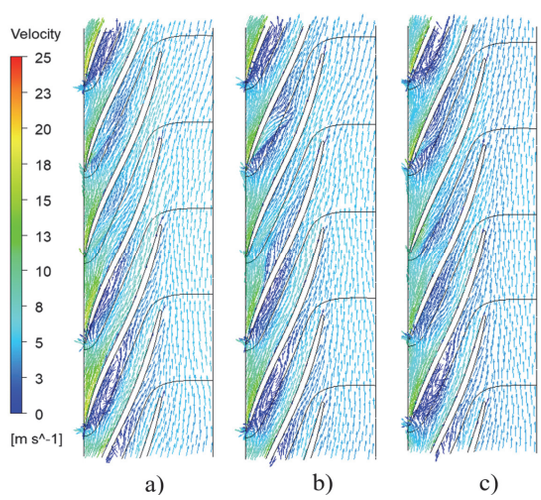

Fig. 14 Velocity vectors in impeller flow passage a) low β_2, b) medium β_2 and c) high β_2 at Q/Q_{BEP} = 0.10 of S–Curve region in turbine mode

the inlet to the outlet in the impeller flow passage in turbine mode. Figs. 14 and 15 show the velocity vectors at Q/Q_{BEP} =0.50 and 0.10 of the S–Curve region in turbine mode, respectively. The recirculation flow is clearly visible at the blade passage at Q/Q_{BEP}=0.50 and 0.10 of the S–Curve region in turbine mode. The recirculation flow in the blade passage at Q/Q_{BEP}=0.10 is significantly higher at high and low β_2 in turbine mode. The recirculation flow and eddies cause shock loss and flow blockage in blade passage.

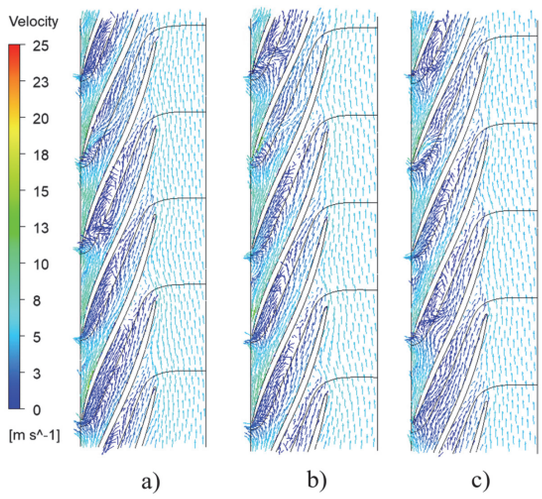

Fig. 15 Velocity vectors in impeller flow passage a) low β_2, b) medium β_2 and c) high β_2 at Q/Q_{BEP} = 0.50 of S-Curve region in turbine mode

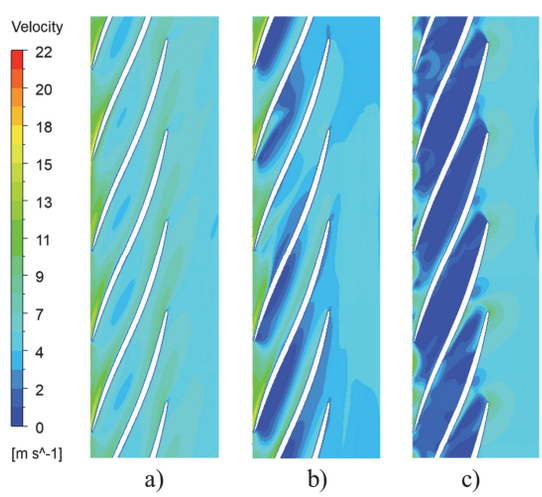

Fig. 16 Velocity contours in medium β_2 impeller in S-Curve region at a) Q/Q_{BEP} = 0.90 turbine mode, b) Q/Q_{BEP} = 0.50 turbine mode and c) Q/Q_{BEP} = 0.10 reverse pump mode

Fig. 16 shows the velocity contours in the blade-to-blade flow passage in the S-Curve region of the medium β_2 impeller. The magnitude of velocity decreases with decreasing flow rates. At Q/Q_{BEP}=0.90, the velocity contours seem smooth without any rotating stall. At Q/Q_{BEP}=0.50 and 0.10, the small velocity magnitude is observed in the blade flow passage. The low-velocity region in the blade passage creates the rotating stall, which develops the blockage effect and reduces the efficiency of the pump turbine in turbine mode. In the S-Curve region, with a decrease in flow rate, the blockage effect is prominent and changes the slope of the speed-flow curves.

Fig. 17 shows the radial velocity vectors in medium β_2 at various flow conditions. At Q/Q_{BEP}=0.90, the bulk of radial velocity is directed inward, and the recirculation flow is minimal. At Q/Q_{BEP} =0.90, the shock loss and recirculation flow are minimal. At Q/Q_{BEP}=0.50, the inward and outward radial velocities are observed. The difference between inward and outward radial velocities creates vortexes and shock loss in turbine mode.

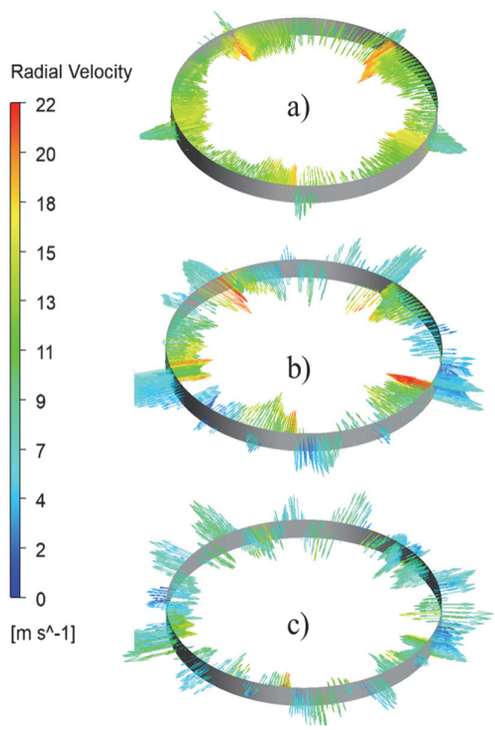

Fig. 17 Velocity vectors in medium β_2 impeller inlet in S-Curve region at a) Q/Q_{BEP} = 0.90 turbine mode, b) Q/Q_{BEP} = 0.50 turbine mode and c) Q/Q_{BEP} = 0.10 reverse pump mode

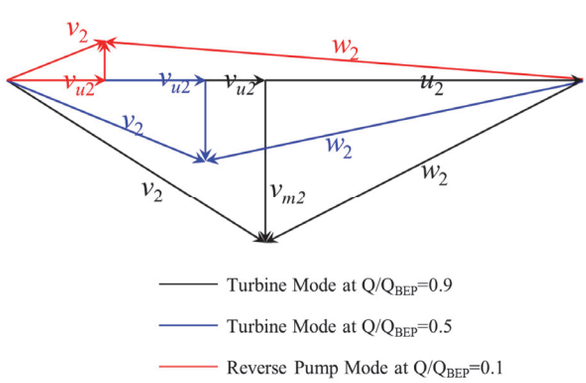

Fig. 18 Velocity triangle in S-Curve region at various operating conditions in pump turbine with medium β_2

In reverse pump mode, the quantity and magnitude of outward radial velocity is higher than inward. The intensity of recirculation flow and vortexes is higher, which causes the flow blockage in the blade passage. Hence, vortexes, recirculation flow, and eddies are common occurrences in the S–Curve region.

Fig. 18 represents the velocity triangle in the pump turbine at various operating conditions. At Q/Q_{BEP}=0.90, the tangential velocity (v_u) and radial velocity (v_m) are comparatively higher. The tangential velocity contributes to the Euler head, and radial velocity directs the flow direction at the impeller inlet in turbine mode. When the flow rate is reduced, the tangential velocity decreases, and radial velocity starts to change the direction from inward to outward direction. Finally, in reverse pump mode, the radial velocity is radially outward.

Fig. 19 shows the velocity contours in the S–Curve region at Q/Q_{BEP}=0.50 with various β_2. The low velocity region is observed in each impeller flow passage at Q/Q_{BEP}=0.50 in the S–Curve region. At low β_2, the area of the low velocity region is comparatively higher than that of medium and high β_2 impellers. It implies that the blockage effect in low β_2 impeller is prominent, and the slope change in the speed–flow curve is more prominent than that of medium and high β_2 impellers.

Fig. 20 shows the change in radial velocity vectors according to the β_2 at Q/Q_{BEP}=0.50 in the S–Curve region of turbine mode. The strength of inward radial velocity is higher for high β_2 compared to low β_2. Fig. 20 indicates that the quantity and magnitude of inward radial velocity are higher in high β_2 impeller. The outward radial velocity is higher for low β_2 at each inlet location in turbine mode. In high β_2 at Q/Q_{BEP}=0.50, the maximum flow is directed inward compared to outward.

It implies that high β_2 is suitable to reduce the outward radial flow in the S–Curve region. The velocity components have the same tendency with various β_2 at LE_{TM}. Finally, Fig. 21 shows the velocity triangle in the S–Curve region at Q/Q_{BEP}=0.50 in turbine mode. The tangential velocity magnitude is higher at a high inlet angle and lower at a low β_2 at

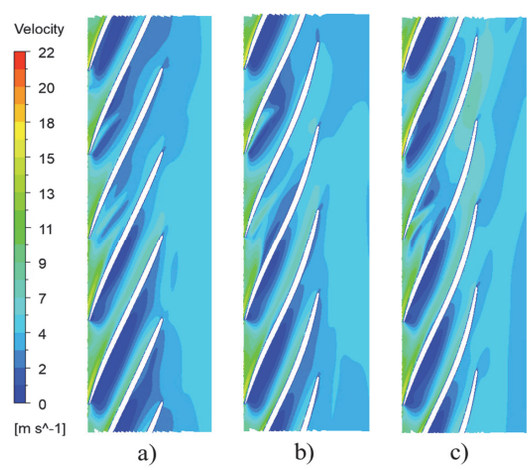

Fig. 19 Velocity contours in impeller a) low β_2, b) medium β_2 and c) high β_2 at Q/Q_{BEP} = 0.50 of S–Curve region in turbine mode

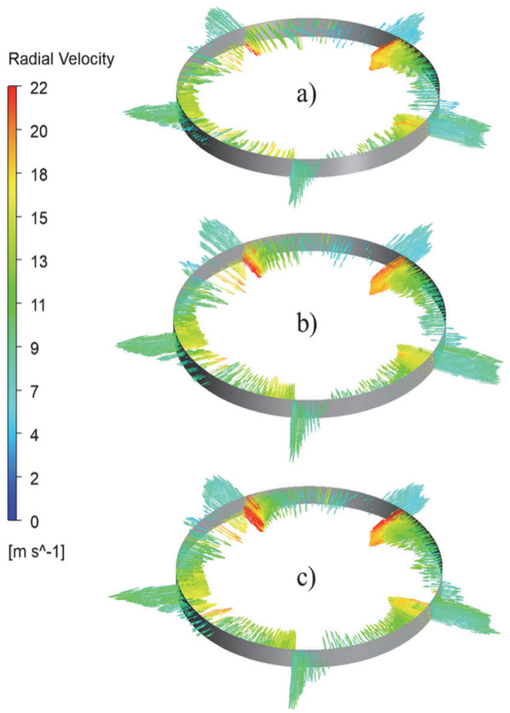

Fig. 20 Velocity vectors in impeller inlet a) low β_2, b) medium β_2 and c) high β_2 at Q/Q_{BEP} = 0.50 of S–Curve region in turbine mode

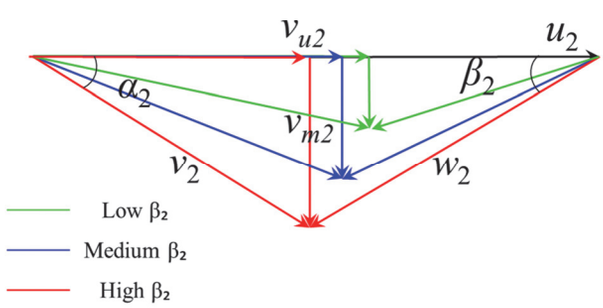

Fig. 21 Velocity triangle at Q/Q_{BEP} = 0.50 of S–Curve region with various impeller inlet angle in turbine mode

Q/Q_{BEP}=0.50 in turbine mode. The radial velocity decreases with a decrease in β_2 in turbine mode. The magnitude of outward radial velocity increases with a reduction in β_2 in turbine mode. The high β_2 is better for reducing the outward radial velocity, and low β_2 is better for tangential velocity.

4. Conclusion

The effect of β_2 in turbine mode is evaluated, and its influence on pump turbine performance in pump and turbine modes. In pump mode, the increase and decrease in β_2 from medium value will decrease efficiency and head in the higher flow rate. Similarly, the change in the inlet angle has no significant effect on the performance of the pump turbine in turbine mode.

The S-Curve region is the hydraulic instability of the pump turbine compared to the usual hydraulic turbine. The intensity of vortexes and recirculation flow in the S-Curve region is very high, which causes the stall and pressure fluctuation in the pump turbine. The numerical analysis was conducted to identify the influence of the impeller β_2 in turbine mode on the S-Curve region. The pressure at the turbine inlet increases with the increase in β_2 in turbine mode. The radial velocity at the turbine inlet contributes to the recirculation flow and shock loss. At the best operating point, the radial velocity direction is radially inward, which reduces the recirculation flow. With decreasing the flow rate, the radial velocity direction changes from radially inward to outward. The tangential and radial velocities are related to the β_2 in turbine mode. The magnitude of the outward radial velocity is higher for low β_2 compared to high β_2 at Q/Q_{BEP} 〈 0.50. When the pump turbine operates in turbine mode at Q/Q_{BEP} 〈 0.50, the S-Curve inception takes place. The blade angle β_2 changes the starting and ending points of the S-Curve region, which influences the inclination of the S-Curve. The low β_2 gives the steeper S-Curve region because of the high magnitude of outward radial velocity. Therefore, the impeller β_2 shows a significant effect on the S-Curve behavior of the pump turbine in turbine mode, and an increase in the β_2 reduces the outward radial velocity magnitude and improves the S-Curve region.

References

(1) Blakers, A., Stocks, M., Lu, B. et al., 2021, "A review of pumped hydro energy storage," Progress in Energy, Vol. 3, No. 2, pp. 022003.

(2) International Hydropower Association, 2023, "2023 World Hydropower Outlook".

(3) Pejovic, S., Krsmanovic, L., Jemcov, R., and Crnkovic, P., 1976, "Unstable Operation of High-Head Reversible Pump-Turbines," 8th IAHR Symposium on Hydraulic Machinery and Cavitation, Leningrad, USSR, pp. 283~295.

(4) Dörfler, P. K., Engineer, A. J., Pendse, R. N., Huvet, P., and Brahme, M. V.,1998, "Stable Operation Achieved on a Single-Stage Reversible Pump-Turbine Showing Instability at No-Load," 19th IAHR Symposium on Hydraulic Machinery and Cavitation, Singapore.

(5) Zhou J. X., Karney B. W., Xu J. C., 2011, "Analytical study on possible self-excited oscillation in S-shaped regions of pump turbines," Proceedings in Mechanical Engineering A – Journal of Power, Vol. 225, No. 8, pp. 1132~1142.

(6) Pejovic S., Zhang Q., F., Karney B., Gajic A., 2011, "Analysis of pump-turbine S instability and reverse water hammer incidents in hydropower systems," 4th International Meeting on Cavitation and Dynamic Problems in Hydraulic Machinery Systems, October 2011, Belgrade, Serbia.

(7) Seidel, U., Koutnik, J. and Martin, G., 2012 "S-Curve characteristic of pump-turbines," HYDRO 2012 Innovative Approaches to Global Challenges, Bilbao, Spain.

(8) Wang, L. Q., Yin, J. L., Jiao, L. et al., 2011, "Numerical investigation on the "S" characteristic of a reduced pump turbine model," Science China Technological Science, Vol. 54, No. 5, pp. 1259~1266.

(9) Zhang, J., Hu, J., Hu. M., et al., 2006, "Study on the Reversible Pump Turbine Closing Law and Field Test," Miami: American Society of Mechanical Engineers, 2006.

(10) Hasmatuchi, V., Farhat M., Roth S., Botero F. and Avellan F., 2011, "Hydrodynamics of a pump turbine at off design conditions in generating mode: an experimental investigation," SHF Conference on Cavitation and Hydraulic Machines, Lausanne, Switzerland.

(11) Senoo, Y. and Yamaguchi, M., 1987, "A study on unstable S-shape characteristic curves of pump turbines at no-flow," Journal of Turbomachine, Vol. 109, pp 72~82.

(12) Olimstad, G., Nielsen, T. and Børresen, B., 2012, "Stability limits of reversible-pump turbines in turbine mode of operation and measurements of unstable characteristics," Journal of Fluids Engineering, Vol. 34, No. 11, pp. 111202-1.

(13) Zanetti, G., Cavazzini, G., and Santolin, A., 2023, "Three-dimensional evolution of the flow unsteadiness in the

S-shape of pump-turbines and its correlation with the runner geometry," Journal of Energy Storage, Vol. 57, pp. 106176.

(14) Jin, F., Wang, H., Luo, Y., Presas, A., Bi, H., Wang, Z., Lin, K., Lei, X. and Yang, X., 2023, "Visualization research of energy dissipation in a pump turbine unit during turbine mode's starting up," Renewable Energy, Vol. 217, pp. 119172.

(15) Wang, T., Xiang, R., Yu, H. and Zhou, M., 2023, "Performance improvement of forward-curved impeller with an adequate outlet swirl using in centrifugal pump as turbine," Renewable Energy, Vol. 204, pp. 67~76.

(16) Yu, H., Wang, T., Dong, Y., Gou, Q., Lei, L. and Liu, Y., 2023, "Numerical investigation of splitter blades on the performance of a forward-curved impeller used in a pump as turbine," Ocean Engineering, Vol. 281, pp. 114721.

(17) Hu, J., Zhao, Z., He, X., Zeng, W., Yang, J. and Yang, J., 2023, "Design techniques for improving energy performance and S-shaped characteristics of a pump-turbine with splitter blades," Renewable Energy, Vol. 212, pp. 333~349.

(18) Cavazzini, G., Houdeline, J., Pavesi, G., Teller, O. and Ardizzon, G., 2018, "Unstable behavior of pump-turbines and its effects on power regulation capacity of pumped-hydro energy storage plants," Renewable and Sustainable Energy Reviews, Vol. 94, pp. 399~409.

(19) Shrestha, U., Singh, P. M. and Choi, Y-D., 2019, "Design and Experimental Analysis on 3kW class Pump Turbine Model for Renewable ESS," KSFM, Vol. 22, No. 4, pp. 19~28.

(20) Kubota, T., 1997, "Hydraulic Design of Francis Pump Turbine," in Hydraulic Design of Hydraulic Machinery, Ashgate Publishing Limited, Wiltshire, pp 465~484.

(21) ANSYS Inc., 2022, "ANSYS CFX documentation ver 2022R2", http://www.ansys.com.

(22) Celik, I. B., Ghia, U., Roache, P. J., Freitas, C. J., Coleman, H. and Raad, P. E., 2008, "Procedure for Estimation and Reporting of Uncertainty Due to Discretization in CFD Applications," Journal of Fluids Engineering, Vol. 130, No. 7, pp. 078001.

(23) Shrestha, U. and Choi, Y-D., 2020, "A CFD-based shape design optimization process of fixed flow passages in a Francis hydro turbine," Processes, Vol. 8, No. 11, pp. 1392.

(24) Shrestha, U. and Choi, Y-D., 2022, "Estimation of Reverse Flow Rate in J-Groove Channel of AJP and SCP Models Using CFD Analysis," Processes, Vol. 10, No. 4, pp. 785.